JAERI-M
9533

INVESTIGATION OF TYPICALITY OF NON-NUCLEAR ROD AND FUEL-CLAD GAP EFFECT DURING REFLOOD PHASE, AND DEVELOPMENT OF A FEM THERMAL TRANSIENT ANALYSIS CODE HETFEM

June 1981

Takashi Sudoh

日本原子力研究所
Japan Atomic Energy Research Institute

この報告書は，日本原子力研究所がJAERI-Mレポートとして，不定期に刊行している研究報告書です．入手，複製などのお問合わせは，日本原子力研究所技術情報部（茨城県那珂郡東海村）あて，お申しこしください．

JAERI-M reports, issued irregularly, describe the results of research works carried out in JAERI. Inquiries about the availability of reports and their reproduction should be addressed to Division of Technical Information, Japan Atomic Energy Research Institute, Tokai-mura, Naka-gun, Ibaraki-ken, Japan.

JAERI-M 9533

Investigation of Typicality of Non-nucelar Rod and Fuel-clad Gap Effect During Reflood Phase, and Development of a FEM Thermal Transient Analysis Code HETFEM

Takashi SUDOH
Division of Reacotr Safety,
Tokai Research Establishment, JAERI
(Reseived May 27, 1981)

The objective of this study are:

1) Evaluate the capability of the electrical heater for simulating the fuel rod during the reflood phase, and
2) To investigate the effect of the clad-fuel gap in the fuel rod on the clad thermal response during the reflood pahse.

A computer code HETFEM which is the two dimensional transient thermal conductivity analysis code utilized a finite element method is developed for analysing thermal responses of heater and fuel rod.

The two kinds of electrical heaters and a fuel rod are calculated with simple boundary conditions.

1) direct heater (former JAERI reflood test heater)
2) indirect heater (FLECHT test heater)
3) fuel rod (15x15 type in Westinghouse PWR)

The conparison of the clad temperature responses shows the quench time is influenced by the thermal diffusivity and gap conductance.

In the conclusion, the ELECHT heater shows atypicality in the clad temperature response and heat releasing rate. But the direct heater responses are similar to those of the fuel rod.

For the gap effect on the fuel rod behavior, the lower gap conductance causes sooner quench and less heat releasing rate.

This calculation is not considered the precursory cooling which is affected by heat releasing rate at near and below the quench front. Therefore two dimensional calculation with heat transfer related to the local fluid conditions will be needed.

Keywords: PWR, LOCA, Reflood, Electric Heater, Pellet-clad Gap, Thermal Response, Simulation Transient Heat Conduction, Finite Element Method, Computer Code.

再冠水実験における電気ヒータの模擬性と燃料と被覆管間のギャップ効果の検討および有限要素法2次元非定常熱伝導解析コード（HETFEM）の開発

日本原子力研究所東海研究所安全工学部
須藤高史

（1981年5月27日受理）

本研究所では，有限要素法を用いた非定常熱伝導解析コードHETFEMを開発し，そのコードにより，直接通電ヒータ，間接型ヒータ，実燃料の3種について1次元解析を行い，電気ヒータの模擬性を検討した。また，実燃料計算では，ギャップ熱伝導率をパラメータに3例の結果を得，ギャップの温度応答に対する効果の検討を行った。

Contents

目　　次

List of Table

List of Figures

1. Introduction

There has been many reflood experiments which were conducted to evaluate thermo-hydraulic pheromena for Loss-of-Coolant Accident (LOCA) in a PWR. For most of these tests[1),2),3)], the nuclear fuel rods were simulated by electric heater rods due to difficulties of the fuel handling and the cost of it. Similarity of the electric heater has been disputed because of the difference of the material thermal properties and the fuel-clad gap effect.

Because there has been few nuclear tests[4),5)] for the reflood plase, the fuel rod responses have not been understood well. The objectives of this study are:

- To evaluate the capability of the electrical heater for simulating the fuel rod during the reflood phase, and
- To investigate the effect of the clad-fuel gap in the fuel rod on the clad thermal responses during reflood phase.

A computer code, HETFEM, is developped to realize the above objectives. The abilities required to this code are to hundle

- a transient conduction problem
- system which contains a gap like as the fuel rod

and

- system which has a complex geometry.

The third item is added to analyse a mechanical clad deformation effect. A finite element method is employed in this code because major characteristics of this method are to calculate a complex geometry system and easy treatment of boundary conditions.

2. Code "HETFEM" Description

Recently, a finite element method has been used for heat transfer problems and fluid flow problems[6),7),8),9)]. Comparing with a finite difference method, a finite element method has a flexibility for a system geometry and boundary conditions, but it requires larger core memory in a computer. After investigating both methods[10)], the finite element method is slelcted. The code HETFEM follows the reference 9 which has a capability of treating a gap conductance.

This section presents method of weighted residuals, numerical formulation and example calculation.

2.1 Development of Method of Weighted Residuals

The partial differential equation and boundary conditions in vector notation for transient heat conduction in a solid are:

$$-\rho c\dot{T} + \underset{\sim}{\nabla}\cdot(\underset{\approx}{k}\cdot\underset{\sim}{\nabla}T) + g = 0 \tag{1}$$

$$-q + \underset{\sim}{n}\cdot\underset{\approx}{k}\cdot\underset{\sim}{\nabla}T = 0 \tag{2}$$

where ρc : heat capacity (density × specific heat capacity)

T : temperature

$\underset{\approx}{k}$: conductivity tensor

g : heat generation rate

q : specified boundary heat flux

$\underset{\sim}{n}$: unit vector, normal (positive outward)

The method of weighted residuals is used to approximate the solution to this problem. The unknowns are determined by making the traial solution and approximately satisfy these equations, not exactly.

Difine the residuals for equations (1) and (2).

$$Ri = \underset{\sim}{\nabla}\cdot(\underset{\approx}{k}\cdot\underset{\sim}{\nabla}T) - \rho c\dot{T} + g \tag{3}$$

$$Rs = -q + \underset{\sim}{n}\cdot\underset{\approx}{k}\cdot\underset{\sim}{\nabla}T \tag{4}$$

Note : ~ represents vector and ≈ represents matrix

The exact solution is obtained when the residual are identically zero. As an approximation to this ideal, the weighted integrals of the residuals are made zero:

$$\iiint_V \omega \cdot R_i \, dV = 0 \tag{5}$$

$$\iiint_S \omega \cdot R_s \, dS = 0 \tag{6}$$

where ω is the weighting function, V is volume and S is surface area.

Substituting equations (3) and (4) into (5) and (6), the integral equations become:

$$\iiint_V \omega \underset{\sim}{\nabla} \cdot (\underset{\approx}{k} \cdot \underset{\sim}{\nabla} T) dV - \iiint_V \omega \rho c \dot{T} dV + \iiint_V \omega g dV = 0 \tag{7}$$

$$\iint_S \omega \cdot q dS = \iint_S \omega (\underset{\approx}{k} \cdot \underset{\sim}{\nabla} T) \cdot \underset{\sim}{n} dS \tag{8}$$

A vector identity gives,

$$\omega (\underset{\sim}{\nabla} \cdot \underset{\sim}{D}) = \underset{\sim}{\nabla} (\omega \underset{\sim}{D}) - (\underset{\sim}{\nabla} \omega) \cdot \underset{\sim}{D} \tag{9}$$

where

$$\underset{\sim}{D} = \underset{\approx}{k} \cdot \underset{\sim}{\nabla} T$$

The substitution of (9) into (7) yields:

$$\iiint_V \underset{\sim}{\nabla} \cdot (\omega \underset{\sim}{D}) dV - \iiint_V (\underset{\sim}{\nabla} \omega) \cdot \underset{\sim}{D} dV - \iiint_V \omega \rho c \dot{T} dV + \iiint_V \omega g dV = 0 \tag{10}$$

From the Gauss divergence theorem and equation (8)

$$\iiint_V \underset{\sim}{\nabla} \cdot (\omega \underset{\sim}{D}) dV = \iint_S (\omega \underset{\sim}{D}) \cdot \underset{\sim}{n} dS = \iint_S \omega q dS \tag{11}$$

Substitution of equation (11) into (10) gives:

$$-\iint_S \omega q dS + \iiint_V (\underset{\sim}{\nabla} \omega) \cdot (\underset{\approx}{k} \cdot \underset{\sim}{\nabla} T) dV + \iiint_V \omega \rho c \dot{T} dV - \iiint_V \omega g dV = 0 \tag{12}$$

The finite element approximation is now made by assuming that the volume can be broken up into a certain number of elements, then the integral equation (12) may be written as follows:

$$\sum_{i=1}^{N} \{ \iiint_{V_i} \underset{\sim}{\nabla} \omega \cdot (\underset{\approx}{k} \cdot \underset{\sim}{\nabla} T) dV + \iiint_{V_i} \omega \rho c \dot{T} dV - \iint_{S_i} \omega q dS - \iiint_{V_i} \omega g dV \} = 0 \tag{13}$$

where V_i is the volume of the i-th element, S_i is the boundary surface area, and N is the total number of elements in the volume.

The variation of the temperature with in each element must be assumed. The usual approach is to assume that the temperature varies linearly within the element. That is:

$$T = \underset{\sim}{\psi}\underset{\sim}{\xi} \tag{14}$$

where T is the local temperature in the element, $\underset{\sim}{\psi}$ is a raw vector representing the spatial temperature variation and $\underset{\sim}{\xi}$ is a column vector of coefficients. If $\underset{\sim}{T}$ is the vector containing the nodal point temperatures of the element, a set of simultaneous equations may be obtained as follows:

$$\underset{\sim}{T} = \underset{\sim}{\lambda}^{*}\underset{\sim}{\xi} \tag{15}$$

then

$$\underset{\sim}{\xi} = \underset{\approx}{\lambda}\underset{\sim}{T} \tag{16}$$

with

$$\underset{\approx}{\lambda} = [\underset{\approx}{\lambda}^{*}]^{-1}$$

Substitution of equation (16) into (14) gives:

$$T = \underset{\sim}{\psi}\underset{\approx}{\lambda}\underset{\sim}{T} \tag{17}$$

If the solutions of equation (1) and (2) are exact, then equation (5) and (6) are satisfied regardless of the choice of the weighting functions. There are several ways for choosing the form of weighting functions, and each choice corresponds to a different criterion in the method of weighted residuals. In this method, a number or different weighting functions are chosen so that the number of equations obtained is equal to the number of unknown. The weighting function is treated as a vector of different functions.

The Galerkin method is selected in this code, then weighting function are taken to be the coefficients of the descrete temperatures as follows.

$$\underset{\sim}{\omega} = (\underset{\sim}{\psi}\underset{\approx}{\lambda})^{T} = \underset{\approx}{\lambda}^{T}\underset{\sim}{\psi}^{T} \tag{18}$$

The required derivatives are:

$$\underset{\sim}{\nabla}T = \underset{\sim}{\psi}' \underset{\approx}{\lambda}\ \underset{\sim}{T} \tag{19}$$

and

$$\underset{\sim}{\nabla}\omega = \underset{\approx}{\lambda}^{T} \underset{\approx}{\psi}'^{T} \tag{20}$$

where prime denotes differentiation.
Substituting the above into equation (13) gives.

$$\sum_{i=1}^{N} [\ \underset{\approx}{K}_i \underset{\sim}{T}_i + \underset{\approx}{C}_i \dot{\underset{\sim}{T}}_i - \underset{\sim}{Q}_i - \underset{\sim}{G}_i\ ] = 0 \tag{21}$$

where

$$\left.\begin{aligned}
\underset{\approx}{K}_i &= \iiint_{V_i} \underset{\approx}{\lambda}_i^{T} \underset{\approx}{\psi}_i'^{T} \underset{\approx}{k}_i \underset{\approx}{\psi}_i' \underset{\approx}{\lambda}_i \, dV \\
\underset{\approx}{C}_i &= \iiint_{V_i} \rho_i c_i \underset{\approx}{\lambda}_i^{T} \underset{\sim}{\psi}_i^{T} \underset{\sim}{\psi}_i \underset{\approx}{\lambda}_i \, dV \\
\underset{\sim}{Q}_i &= \iint_{S_i} \underset{\approx}{\lambda}_i^{T} \underset{\sim}{\psi}_i^{T} \underset{\sim}{q}_i \, dS \\
\underset{\sim}{G}_i &= \iiint_{V_i} \underset{\approx}{\lambda}_i^{T} \underset{\sim}{\psi}_i^{T} \underset{\approx}{g}_i \, dV
\end{aligned}\right\} \tag{22}$$

with the term $\dot{T}$ approximated as:

$$T = \underset{\sim}{\psi} \underset{\approx}{\lambda} \dot{\underset{\sim}{T}} \tag{23}$$

Two Dimensional Formulation

In some cases, a three node triangular element is used, and nodal point locations are difined with the global (x, y) coodinate system, as shown in Fig. 2.1.

If the temperature within the element varies linearly between the nodes, then the temperature is expressed the spatial variation of temperature in the element:

$$T = [1\ x\ y]\ \underset{\sim}{\xi} \tag{26}$$

Note : upper subscript, T, denotes transposed matrix

Using the above equation at each node, a set of simultaneos equations is obtained:

$$\begin{bmatrix} T_i \\ T_j \\ T_k \end{bmatrix} = \begin{bmatrix} 1 & x_i & y_i \\ 1 & x_j & y_j \\ 1 & x_k & y_k \end{bmatrix} \underset{\sim}{\xi} \tag{27}$$

Hence

$$\underset{\sim}{\xi} = \begin{bmatrix} 1 & x_i & y_i \\ 1 & x_j & y_j \\ 1 & x_k & y_k \end{bmatrix}^{-1} \underset{\sim}{T} \tag{28}$$

where

$$\underset{\sim}{T} = \begin{bmatrix} T_i \\ T_j \\ T_k \end{bmatrix}$$

Substituting equation (28) into (26)

$$T = \underset{\sim}{\psi}\underset{\sim}{\lambda}\underset{\sim}{T} \tag{29}$$

where

$$\underset{\sim}{\psi} = [1 \; x \; y] \tag{30}$$

and

$$\underset{\sim}{\lambda} = \begin{bmatrix} 1 & x_i & y_i \\ 1 & x_j & y_j \\ 1 & x_k & y_k \end{bmatrix}^{-1} \tag{31}$$

The dilivative $\underset{\sim}{\psi}'$ is

$$\underset{\sim}{\psi}' = \begin{bmatrix} \frac{\partial \psi}{\partial x} \\ \frac{\partial \psi}{\partial y} \end{bmatrix} = \begin{bmatrix} 0 & 1 & 0 \\ 0 & 0 & 1 \end{bmatrix} \tag{31}$$

and

$$\underset{\sim}{\lambda} = \begin{bmatrix} 1 & x_i & y_i \\ 1 & x_j & y_j \\ 1 & x_k & y_k \end{bmatrix} = \frac{1}{2A} \begin{bmatrix} a_i & a_j & a_k \\ b_i & b_j & b_k \\ c_i & c_j & c_k \end{bmatrix} \tag{32}$$

where

$$a_i = x_j y_k - x_k y_j \qquad a_j = x_k y_i - x_i y_k \qquad a_k = x_i y_j - x_j y_i$$

$$b_i = y_i - y_k \qquad b_j = y_k - y_i \qquad a_k = y_i - y_j$$

$$c_i = x_k - x_j \qquad c_j = x_i - x_k \qquad a_k = x_j - x_i$$

$A = \frac{1}{2}(x_j y_k - x_k y_j)$: area of triangle element

Substituting equations (31) and (32) into equations (22), followings are obtained.

∘ Conductivity term

Assume that conductivity (k) is constant in a small element and thickness which is normal to X-Y plane is unit

$$\underset{\sim}{K}_{\ell} = k_{\ell} \iiint_{V_{\ell}} \underset{\sim}{\lambda}_{\ell}^{T} \underset{\sim}{\psi}_{\ell}^{T} \underset{\sim}{\psi}_{\ell}' \underset{\sim}{\lambda} \, dV$$

$$= \frac{k_{\ell}}{4A} \begin{bmatrix} b_i^2 + c_i^2 & b_i b_j + c_i c_j & b_i b_k + c_i c_k \\ b_j b_i + c_j c_i & b_j^2 + c_j^2 & b_j b_k + c_j c_k \\ b_k b_i + c_k c_i & b_k b_j + c_k c_j & b_k^2 + c_k^2 \end{bmatrix} \tag{33}$$

∘ Capacitance term

Assume that material propaties are constant in a element.

$$\underset{\sim}{C}_{\ell} = \rho_{\ell} c_{\ell} \iiint_{V_{\ell}} \underset{\sim}{\lambda}_{i}^{T} \underset{\sim}{\psi}_{i}^{T} \underset{\sim}{\psi}_{i} \underset{\sim}{\lambda}_{i} \, dV$$

$$= \frac{\rho_{\ell} c_{\ell}}{12A} \begin{bmatrix} 2 & 1 & 1 \\ 1 & 2 & 1 \\ 1 & 1 & 2 \end{bmatrix} \tag{34}$$

∘ Convection term

a) heat flux

Node i and j side of a element is a boundary of the system and heat transfers through this side. Assume that heat flux varies lineary on this side.

$$q(x,y) = \underset{\sim}{\psi} \, \underset{\sim}{\lambda} \, \underset{\sim}{q}$$

$$\underset{\sim}{Q}_{\ell} = \iint_{S_{\ell}} \underset{\sim}{\lambda}^{T} \underset{\sim}{\psi}^{T} \underset{\sim}{\psi} \, \underset{\sim}{\lambda} \, \underset{\sim}{q} \, dS$$

$$= L \begin{bmatrix} \frac{1}{3} q_i + \frac{1}{6} q_j \\ \frac{1}{6} q_i + \frac{1}{3} q_j \end{bmatrix} \tag{35}$$

where

L : Length between nodes i and j

$\underset{\sim}{q}$: node heat flux

b) convection

heat flux is given,

$$q(x,y) = h\{T(x,y) - T_\infty(x,y)\}$$

Assuming that heat transfer coefficient is constant in this side and surface temperature and environment temperature vary lineary along this side.

$$q(x,y) = h\{\underset{\sim}{\psi}\underset{\sim}{\lambda}\underset{\sim}{T} - \underset{\sim}{\psi}\underset{\sim}{\lambda}\underset{\sim}{T}_\infty\}$$

where $\underset{\sim}{T}$ and T_∞ are node and environment temperatures, respectively then

$$Q_\ell = hL \iint_{S_\ell} \underset{\sim}{\lambda}^T \underset{\sim}{\psi}^T (\underset{\sim}{\psi}\underset{\sim}{\lambda}\underset{\sim}{T} - \underset{\sim}{\psi}\underset{\sim}{\lambda}\underset{\sim}{T}_\infty)$$

$$= hL\begin{bmatrix} \frac{1}{3} & \frac{1}{6} \\ \frac{1}{6} & \frac{1}{3} \end{bmatrix}\begin{bmatrix} T_i \\ T_j \end{bmatrix} - hL\begin{bmatrix} \frac{1}{3}T_{\infty i} + \frac{1}{6}T_{\infty i} \\ \frac{1}{6}T_{\infty i} + \frac{1}{3}T_{\infty i} \end{bmatrix} \qquad (36)$$

∘ Gap heat transfer

When small gap exists between elements and heat transfers between node i and j side and node i′ and j′ side, the boundary condition of the heat transfer, described above, is used to connect these elements. At the element I which contains nodes i and j, convection term is expressed,

$$\underset{\sim}{Q}_I = h_g L\begin{bmatrix} \frac{1}{3} & \frac{1}{6} \\ \frac{1}{6} & \frac{1}{3} \end{bmatrix}\begin{bmatrix} T_i \\ T_j \end{bmatrix} - h_g L\begin{bmatrix} \frac{1}{3} & \frac{1}{6} \\ \frac{1}{6} & \frac{1}{3} \end{bmatrix}\begin{bmatrix} T_{i'} \\ T_{j'} \end{bmatrix}$$

and at the another element side,

$$\underset{\sim}{Q}_{II} = h_g L\begin{bmatrix} \frac{1}{3} & \frac{1}{6} \\ \frac{1}{6} & \frac{1}{3} \end{bmatrix}\begin{bmatrix} T_{i'} \\ T_{j'} \end{bmatrix} - h_g L\begin{bmatrix} \frac{1}{3} & \frac{1}{6} \\ \frac{1}{6} & \frac{1}{3} \end{bmatrix}\begin{bmatrix} T_i \\ T_j \end{bmatrix}$$

Above two equations are summed up, then

$$\underset{\sim}{Q}_{I,II} = \begin{bmatrix} \frac{1}{3} & \frac{1}{6} & -\frac{1}{3} & \frac{1}{6} \\ \frac{1}{6} & \frac{1}{3} & -\frac{1}{6} & \frac{1}{3} \\ \frac{1}{3} & \frac{1}{6} & -\frac{1}{3} & \frac{1}{6} \\ \frac{1}{6} & \frac{1}{3} & -\frac{1}{6} & \frac{1}{3} \end{bmatrix} \begin{Bmatrix} T_i \\ T_j \\ T_i' \\ T_j' \end{Bmatrix} \tag{37}$$

∘ Heat generation term

Heat generation rate in a element is given, when linear variation is assumed

$$g(x,y) = \underset{\sim}{\psi}\underset{\sim}{\lambda}\underset{\sim}{g}$$

where

$\underset{\sim}{g}$ is the heat generation rates at the nodal points

then

$$\underset{\sim}{G}_{\ell} = \iiint_{V_{\ell}} \underset{\sim}{\lambda}^{T}\underset{\sim}{\psi}^{T}\underset{\sim}{\psi}\,\underset{\sim}{\lambda}\,\underset{\sim}{g}\,dV$$

$$= \frac{A}{12}\begin{bmatrix} 2g_i + g_j + g_k \\ g_i + 2g_j + g_k \\ g_i + g_j + 2g_k \end{bmatrix} \tag{38}$$

The equations for an axisymmetric cylinder coordination are also obtained easily with the same manor as for a global coordination.

2.2 Method of Numerical Solution

The model which has been described is expressed as

$$\underset{\sim}{K}\underset{\sim}{T} + \underset{\sim}{C}\dot{\underset{\sim}{T}} - \underset{\sim}{Q} = 0 \tag{39}$$

If the subscript p is used as a counter on time and Δt is a time increment, following equations are obtained from equation (39).

$$\underset{\sim}{K}\underset{\sim}{T}_p + \underset{\sim}{C}\dot{\underset{\sim}{T}}_p - \underset{\sim}{Q}_p = 0$$

$$\underset{\sim}{K}\underset{\sim}{T}_{p+1} + \underset{\sim}{C}\underset{\sim}{T}_{p+1} - \underset{\sim}{Q}_{p+1} = 0$$

becomes

$$\underset{\sim}{K}(\underset{\sim}{T}_{p+1} + \underset{\sim}{T}_p) + \underset{\sim}{C}(\dot{\underset{\sim}{T}}_{p+1} + \dot{\underset{\sim}{T}}_p) = \underset{\sim}{Q}_{p+1} + \underset{\sim}{Q}_p \tag{40}$$

The Crank-Nicolson formulation of which temperature change in a time step is given as an average of differentiations with respect to

time at p and p+1 is employed

$$\underset{\sim}{T}_{p+1} = \underset{\sim}{T}_p + \frac{\Delta t}{2}(\dot{\underset{\sim}{T}}_{p+1} + \dot{\underset{\sim}{T}}_p)$$

substitute this to equation (40)

$$\frac{1}{2}\underset{\approx}{K}(\underset{\sim}{T}_{p+1} + \underset{\sim}{T}_p) + \frac{1}{\Delta t}\underset{\approx}{C}(\underset{\sim}{T}_{p+1} - \underset{\sim}{T}_p) = \frac{1}{2}(\underset{\sim}{Q}_{p+1} + \underset{\sim}{Q}_p)$$

then

$$(\underset{\approx}{K} + \frac{2}{\Delta t}\underset{\approx}{C})\underset{\sim}{T}'_{p+1} = \frac{2}{\Delta t}\underset{\approx}{C}\underset{\sim}{T}_p + \frac{1}{2}(\underset{\sim}{Q}_{p+1} + \underset{\sim}{Q}_p) \qquad (41)$$

where

$$\underset{\sim}{T}'_{p+1} = \frac{1}{2}(\underset{\sim}{T}_{p+1} + \underset{\sim}{T}_p) \qquad (42)$$

In the equation (41), unknown is only $\underset{\sim}{T}'_{p+1}$. After solving equation (42), new time step temperature vector is obtained from modified equation (42)

$$\underset{\sim}{T}_{p+1} = 2\underset{\sim}{T}'_{p+1} - \underset{\sim}{T}_p$$

2.3 Computer Program

The code HETFEM is written in the FORTRAN IV program language for the FACOM-230-75 in JAERI. This section describes an outline of the HETFEM code.

The brief structure of the code is shown in Fig. 2.2. The element generation and node numbering is performed at first by input. For a cylinder and slab geometry, auto-generation and numbering is available by inputting locations of deviders for each axis. The input manual is detailed in Appendix.

After each element matrixes and vectors are calculated, the matrixes and vecter for the total system, $\underset{\approx}{K}$, $\underset{\approx}{C}$ and $\underset{\sim}{Q}$ or $\underset{\sim}{T}$ are assembled. Boundary conditions are accounted for by suitable modifications of the matrixes and vectors. A band matrix is employed to store these matrixes. Then a Gausian elimination is used for the direct solution of the matrix equation. Then the calculated results, temperatures and heat fluxes, are printed out. A plot routine is also available.

2.4 Example calculation

To assure the developed code, HETFEM, a simple transient cases are calculated, and results of them are compared with analytical solutions. One of these comparisons is presented below.

A steel slab which is 20 mm in thickness is initially kept at 900°C, then both surface temperature is suddenly reduced to 100°C in a transient.

An analytical solution[11] is expressed

$$\theta = \theta_0 - (\theta_0 - \theta_s) \sum_{n=0}^{\infty} (-1)^n \{ \mathrm{erfc} \frac{(2n+1)d+x}{2\sqrt{at}} + \mathrm{erfc} \frac{(2n+1)d-x}{2\sqrt{at}} \}$$

where

θ_0 : initial temperature (900°C)

θ_s : surface temperature (100°C)

d : one half of thickness (10mm)

x : distance from slab center

a : thermal diffusivity (0.045 m^2/h)

The HETFEM code is two dimensional analysis code, then the model, shown in Fig. 2.3, is used. In this case, the left hand side is adiabatic, and right hand side surface is maintained at 100°C after initialization. The both calculation results are shown in Fig. 2.4. The HETFEM result agrees very well to the analytical result. Good agreements are also obtained by other comparisons which are not shown in this report.

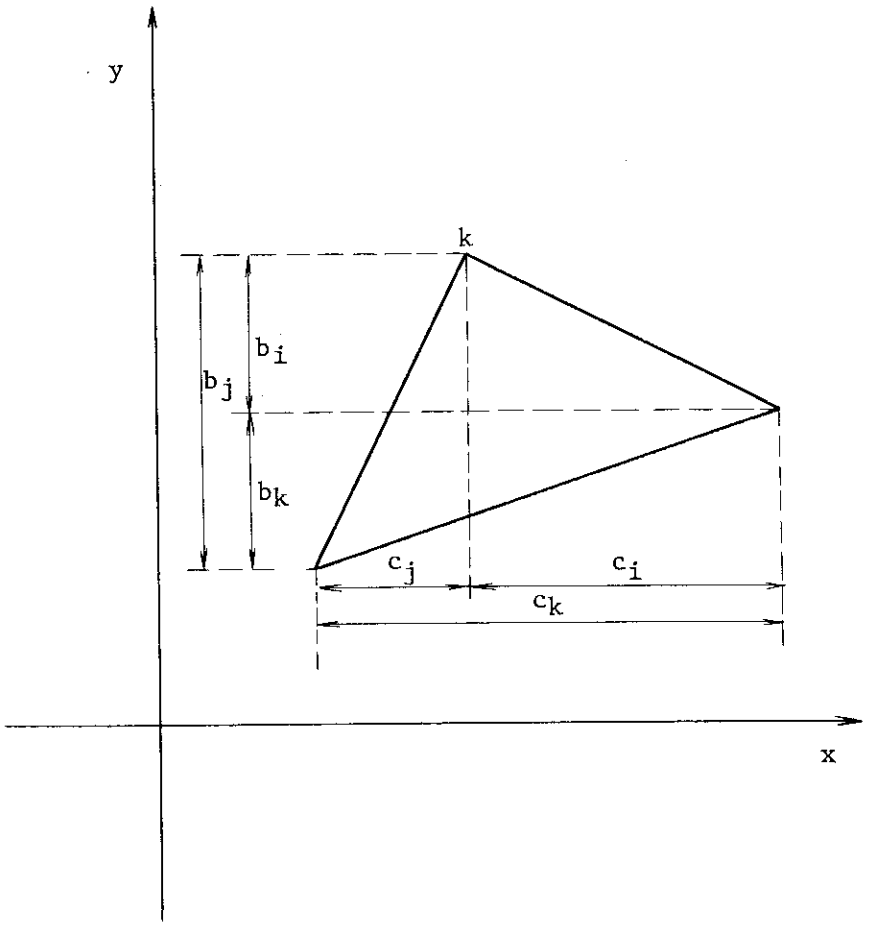

Fig. 2.1 Triangular element on a X-Y plane

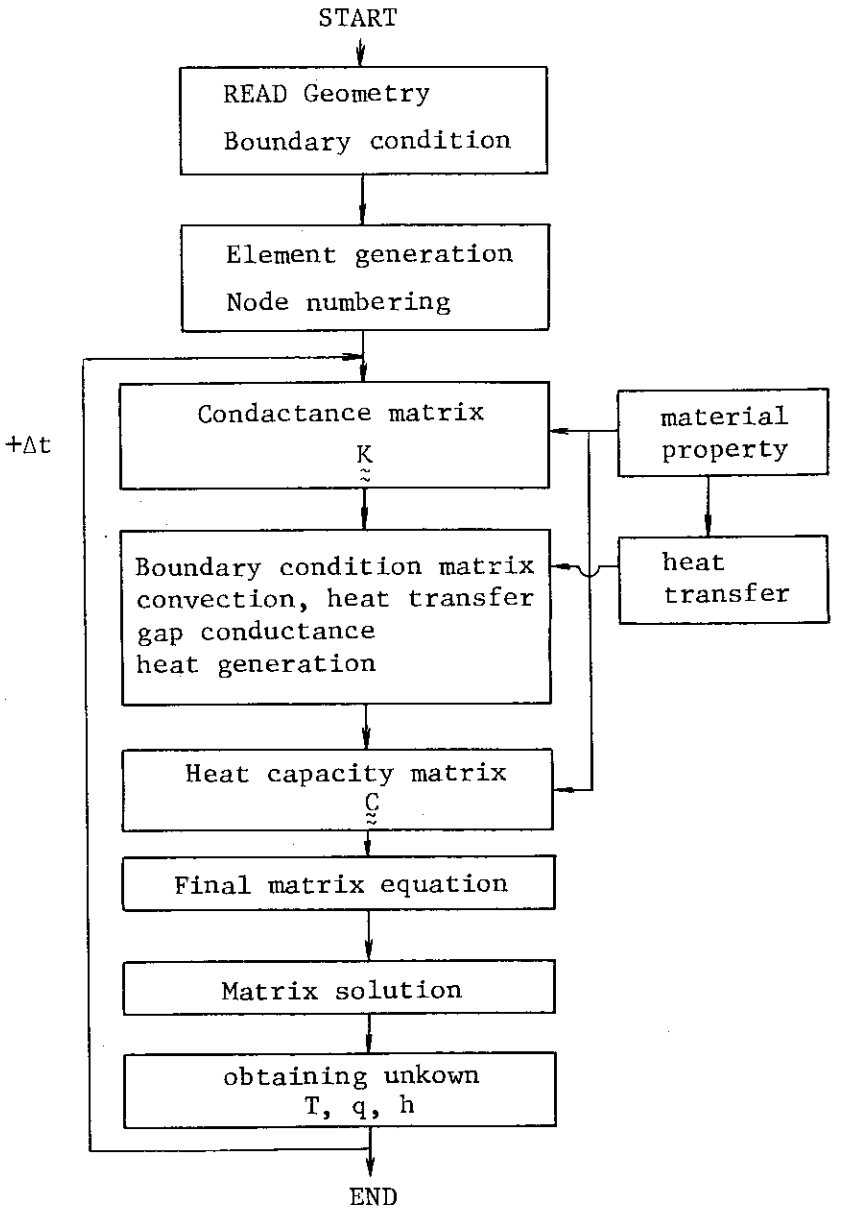

Fig. 2.2 HETFEM schematic diagram

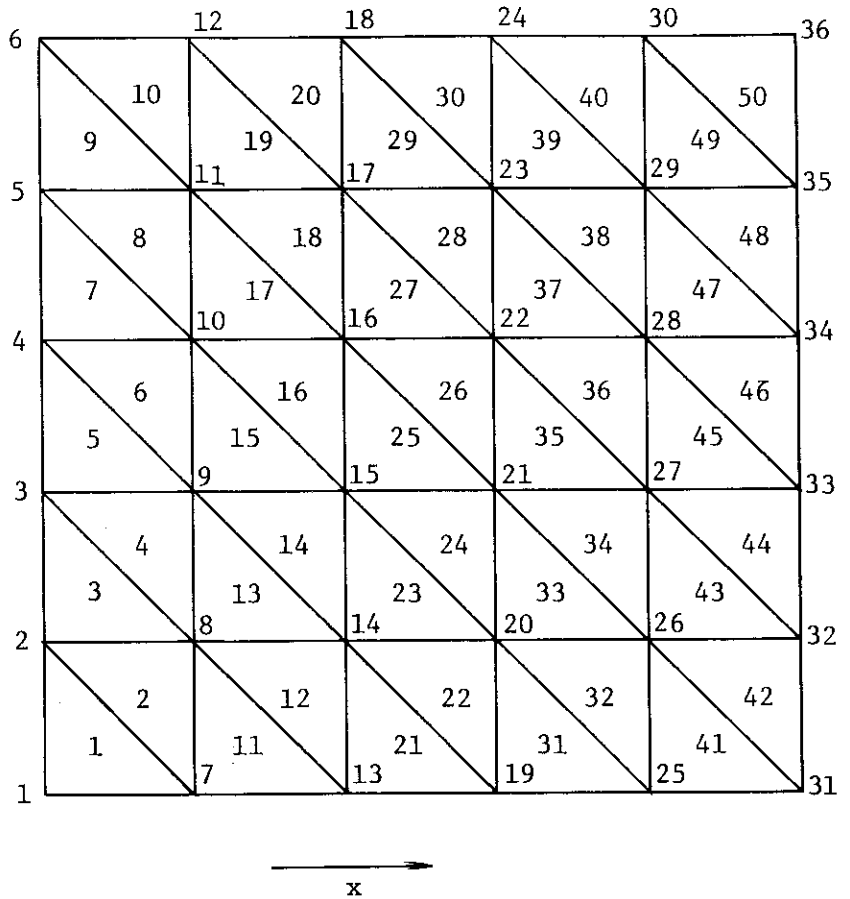

Fig. 2.3 Mesh model of the example case

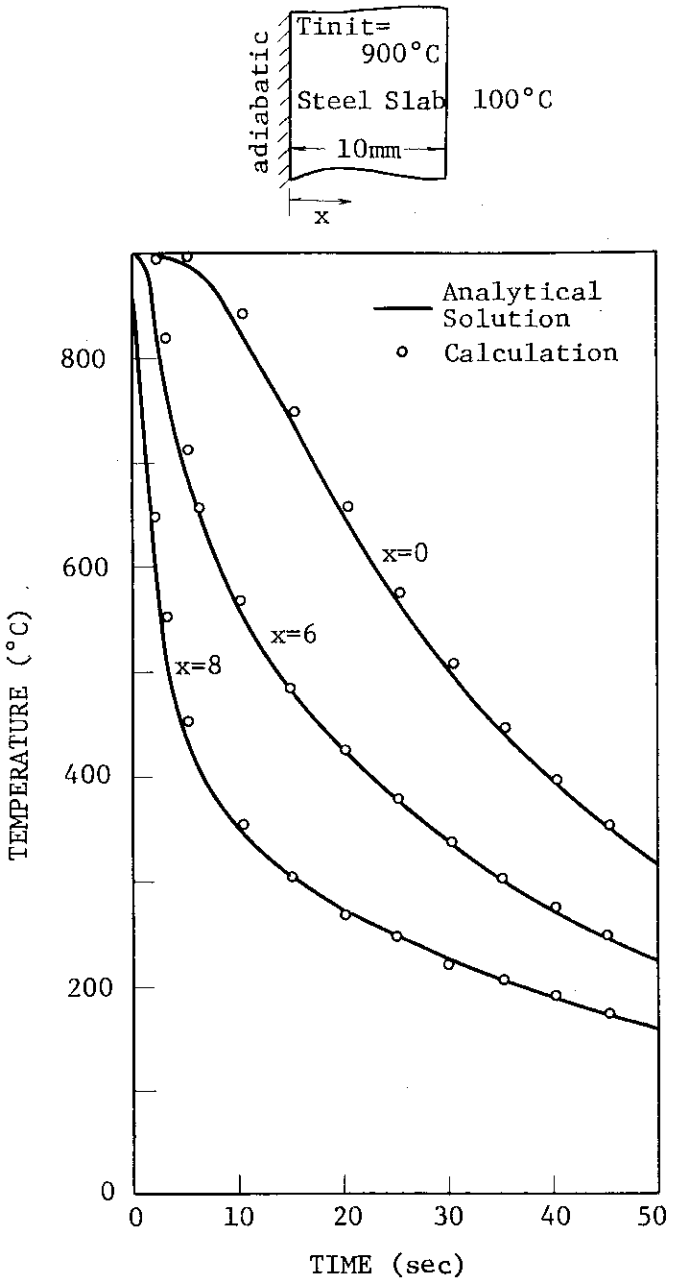

Fig. 2.4 Comparison of HETFEM result with analytical solution

3. Investigation of Typicality of Non-nuclear Rod and Fuel-clad Gap Effect of Nuclear Rod on Clad Thermal Response

The heat transfer above the quench front depends on mixture flow of steam and water droplet, and this fluid condition in the core is affected by the heat releasing rate at near and below the quench front. At the quench front, heat transfer changes drastically from low precursory cooling to high transient boiling cooling. In such a case, wall surface heat transfer is subjected to the heat conduction inside of the wall.

Consequently, material thermal properties which influence the clad thermal response and heat releasing rate are very important during reflood phase.

After verifing the HETFEM, thermal responses of heater rods and fuel rod are calculated by this code to investigate the similarity of the non-nuclear rod to the fuel rod and to evaluate the fuel-clad gap effect during the reflood phase.

The heat transfer during reflood phase is too complex to consider in this code. Then, assuming a boiling curve which is obtained from observation of the JAERI small scale reflood test[1], material thermal property effect is investigated by one dimensional calculation.

Three types of rods were calculated,

1. Direct heater : This had been used for the small-scale reflood test[1] in JAERI.
2. Indirect heater : FLECHT heater[3]
3. Nuclear fuel pin : 15 × 15 type rod in a Westinghouse PWR[12]. Gap conductance is a parameter.

These rods geometries are shown in Fig. 3.1. The clad thicknesses of them are nearly same, though the direct heater has a little smaller diameter than other's.

Thermal properties of materials are given in Table 3.1.

3.1 Calculation Model

The HETFEM models are shown in Fig. 3.2. The model of the direct heater consists of 41 nodes and 52 elements on the r-z coodinates. Heat is generated in the clad. For the FLECHT heater, the second layer from the left hand side, Nichrome, generates heat while the nuclear rod

generates heat in the UO_2 pellet. The fuel rod has the gap between the pellet and clad. There are 41 nodes and 60 elements for the FLECHT heater, and 41 nodes and 52 elements for the fuel rod. The gap conductance during reflood phase has not been known well, then each value of 500, 1,000 and 5000 kcal/m^{2}hr°C is selected for the fuel rod calculation. The initial temperature of each rod is a flat distribution at 800°C, and linear power is 2 KW/m which is generated in the clad for the direct heater, in the nichrome element for the FLECHT heater and in the fuel pellet for the nuclear rod.

The heat transfer on the surface of the clad is assumed as described below and shown in Fig. 3.3. These assumptions are based on the observation of the results of the small reflood test[1)] in JAERI. The heat transfer coefficient is a constant value of 100 Kcal/m^{2}hr°C where the clad temperature is above 700°C. Then heat transfer coefficient is given by the following equation[13)],

$$h_c = 0.62 \left[\frac{\lambda^3 g \rho_g (\rho_\ell - \rho_g) H_{fg} g_c}{L \mu_g (T_w - T_{sat})} \right]^{1/4}$$

and radiation heat transfer is also considered in this mode. When the clad temperature reaches T_2, 500°C, the quench initiates at a constant heat flux, 2×10^6 Kcal/m^{2}hr. Then the heat transfer mode changes to nucleate boiling when heat flux of it decreases to 2×10^6 Kcal/m^{2}hr. Heat flux of the nucleate boiling is obtained by Jens-Lottes equation.

$$q^{1/4} = \frac{\Delta T_{sat}}{0.81} e^{P/63}$$

3.2 Results and Discussion

The calculated temperature responses of the direct heater, indirect heater and fuel rod with a 1,000 kcal/m^{2}hr°C gap conductance are shown in Fig. 3.4. Though the general trend of them is similar due to the same heat transfer curve used in the models, but the temperature decreasing rates and quench times of the rods are different. The temperature difference between the center and clad in the fuel rod is the greatest. The thermal resistance in the gap which reduces heat transfer from the fuel to the clad maintains the center temperature high. And the heat capacitance of the Zr-4 clad is relatively small, as given in Table 3.1.

These reduced heat transfer rate from the fuel to the clad and low stored energy in the clad allow the sooner clad cooling. Then the difference of the center and clad temperature in the fuel rod is greater than that of others, and as a result, the quench time of it is the fastest.

The FLECHT heater shows the smallest temperature difference between the clad surface and the center of the rod due to a higher thermal conductivity of the boron nitride in the heater and a greater heat capacity in unit length, given in Table 3.1, than those of the direct heater. Much heat must be transfered from the insulator and the heater element to the clad then to the fluid before quenching clad. This causes the lowest temperature decreasing rate of the clad and also the slowest quench for the FLECHT heater.

The calculated temperature responses of the fuel rod are shown in Fig. 3.5. The parameter of them is the value of the clad-fuel gap conductances. When the gap conductance is smaller, the clad temperature decreases quicker even in the low precursory cooling phase, while the center temperature remains high. And it quenches faster. For the higher gap conductance fuel rod, the clad temperature decreasing rate is smaller and the center temperature is closer to the clad temperature. This shows that greater heat release is needed for the rod with higher gap conductance before the clad surface reaches a quench temperature. On the contrary, for the rod with lower gap conductance, the clad can reach a quench temperature by releasing only stored energy of itself and a small amount of heat transfered from the pellets.

Heat releasing rates after quenching are shown in Fig. 3.6. Time is refered after quenching. The heat flux is low during the precursory cooling phase before quenching. Then heat flux reaches maximum at the quench temperature. When a nucleate boiling replaces a transient boiling, heat flux decreases.

The heat transfer near and below the quench front may affect the fluid conditions which control heat transfer coefficients above the quench front. This precursory cooling is imprortant for the clad peaking temperature and quench temperature. For the FLECHT heater, the duration of the transient boiling is longer than others and also nucleate boiling heat flux is higher within 3 or 4 sec after the quench. For the fuel rod and direct heater, the nucleate boiling takes the place of the transient boiling at a very short time after quenching, then heat flux

ruduces sharply, but it is a little higher than that of the FLECHT heater after about 4 sec. This shows that the stored energy in the FLECHT heater is released from the clad within a short period after the quench while the fuel rod releases only stored energy in the clad at the quench front and the stored energy in the pellet is transfered gradually to the clad and released slowly after the quench. Lower gap conductance fuel rod shows this trend remarkably. This results indicate that the heat releasing rates after the quench are different between the FLECHT heater and the fuel rod. The heat releasing rate of the direct heater is very similar to that of the fuel rod due to low conductivity of the filler material, magnesia oxide.

Because the reflood phenomena is controled by many parameters which may interact each other, this study is not enough to evaluate the non-nuclear heater typicality or pellet-clad gap conductance effect during the reflood phase.

Experiments will be required to evaluate the gap conductance effect on the precursory cooling and the quench, and two dimensional code calculations of which heat transfer is related to the fluid condition will be needed in the future.

Table 3.1 Thermal properties of rod materials

item / type	material	heat capacity ($kcal/m^3°C$)	conductivity ($kcal/mhr°C$)	volume in unit length ($\times10^{-6}$ m^3/m)	heat capacitance in unit length ($kcal/m°C$)
direct heater	type 316	923	14	18.7	0.0596
	MgO	624	0.64	67.9	
FLECHT heater	type 347	958	17.8	19.37	0.0722
	BN	740	11	62.56	
	Nichrome	888	10	8.32	
fuel rod	Zr-4	524	15.6	19.6	0.0623
	UO_2	767	3.81	67.8	

Note

at room temperature

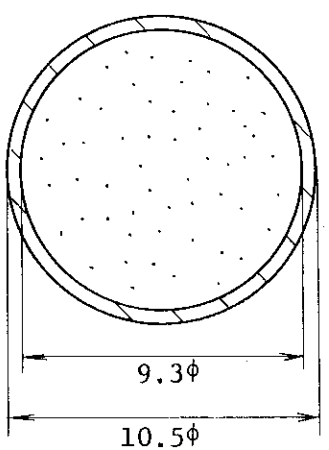

Material Clad : type 316

Filler : MgO

Direct heater

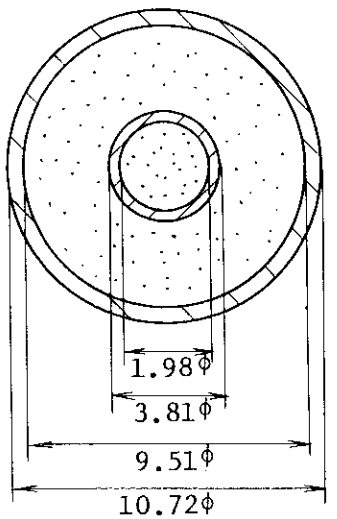

Material Clad : type 347

Element : Nichrome

Insulator : BN

FLECHT heater

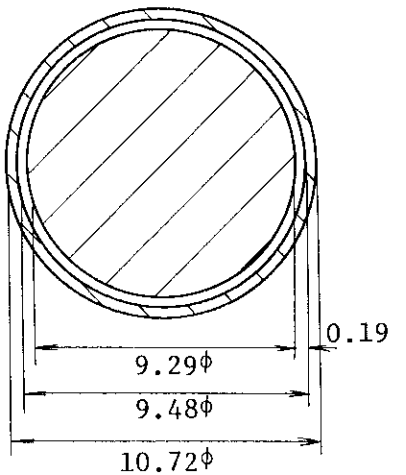

Material Clad : Zr-4

Fuel : UO_2

Reactor fuel

Fig. 3.1 Heaters and fuel rod geometry

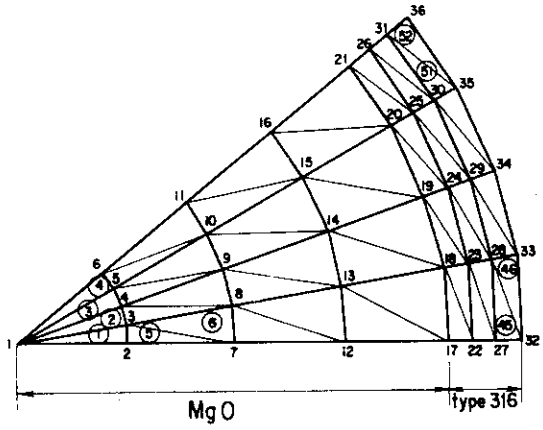

Direct heater

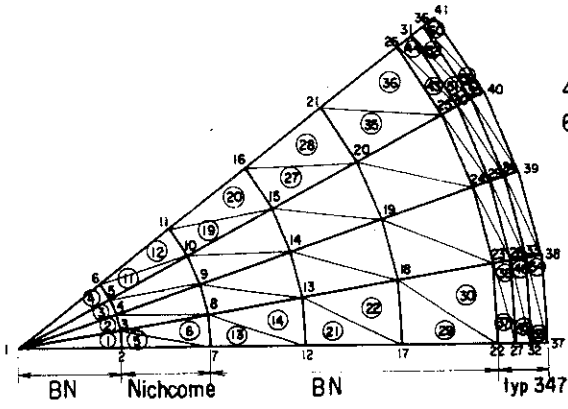

FLECHT heater

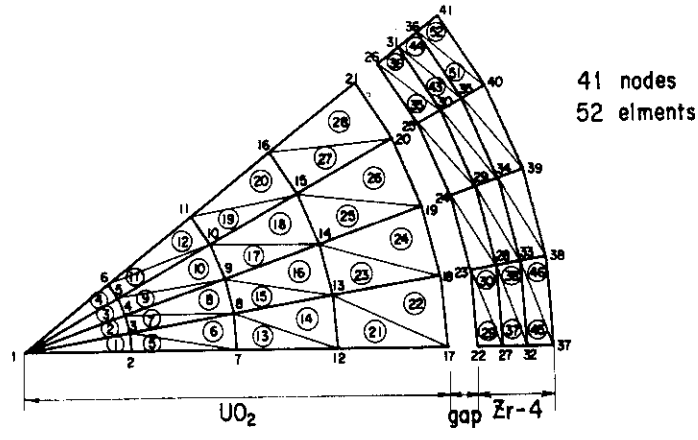

Reactor fuel rod

Fig. 3.2 HETFEM models for each rod

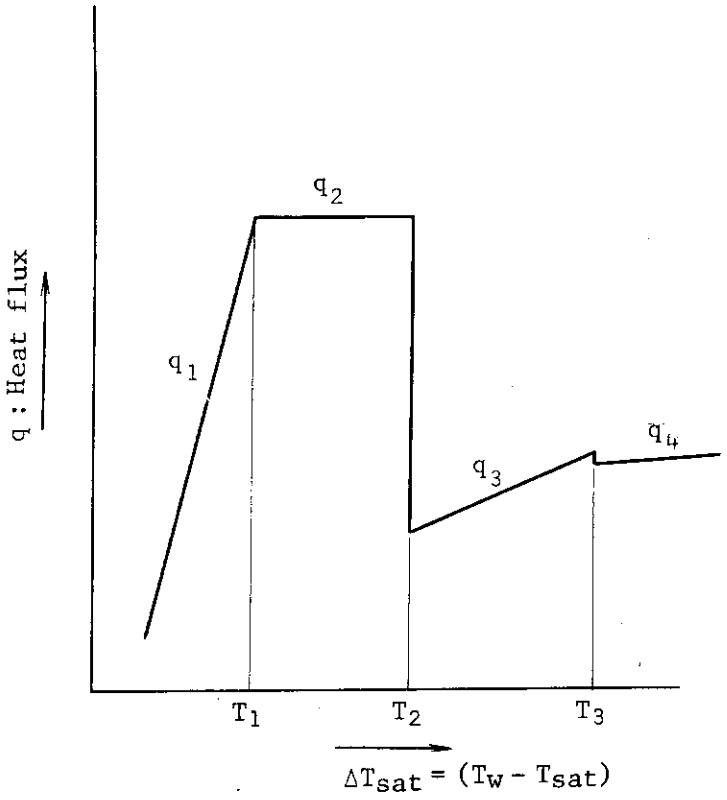

Fig. 3.3 Heat transfer curve model

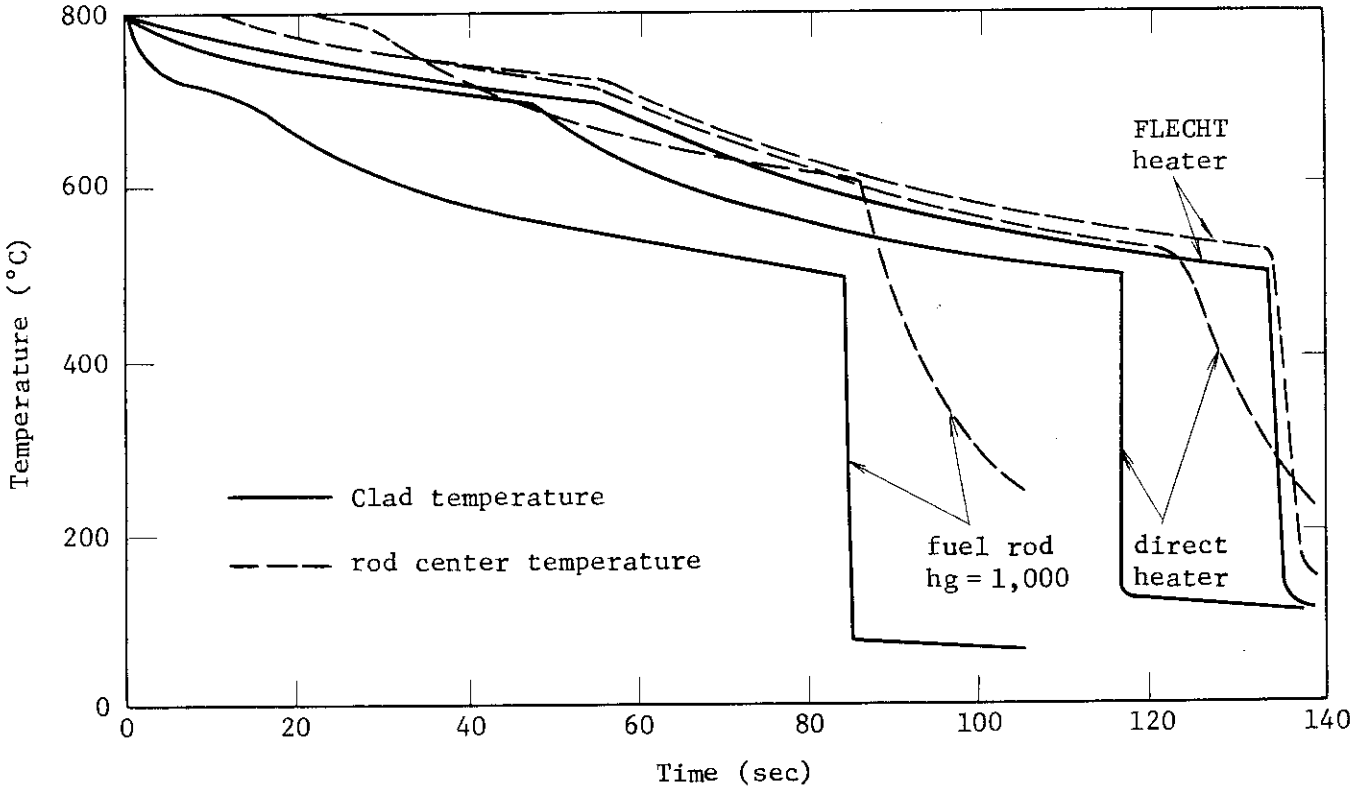

Fig. 3.4 Calculated temperature response of direct heater, FLECHT heater and fuel rod.

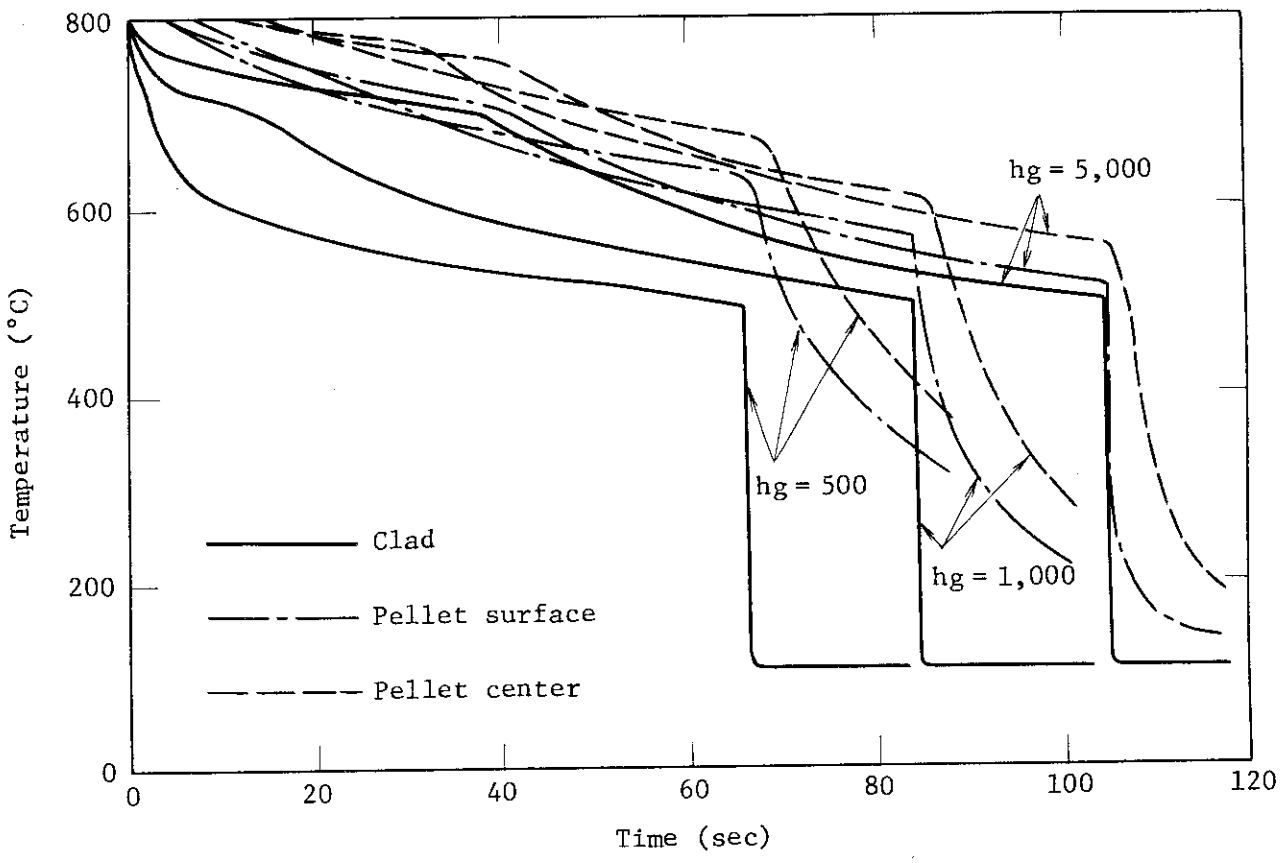

Fig. 3.5 Calculated temperature responses of fuel rod with gap conductance 500, 1000 and 5000 kcal/m^{2}h.

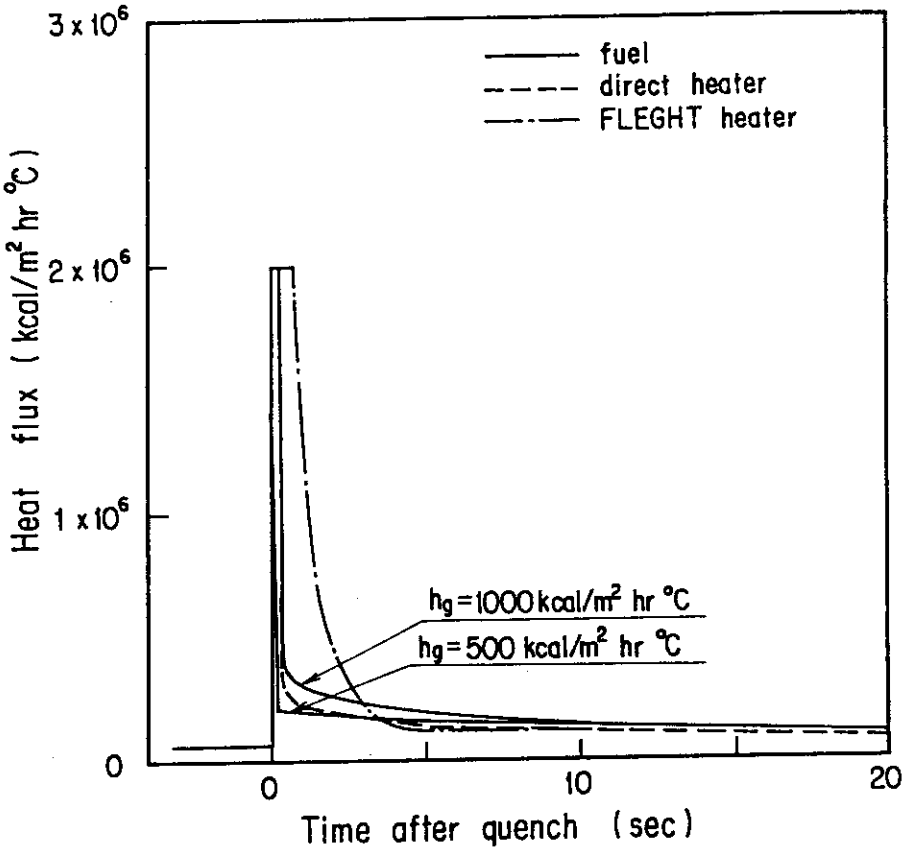

Fig. 3.6 Heat release rate after quench

4. Conclusions

The HETFEM code for analysing the transient heat conduction has been developped. This code employed a finite element method.

The comparisons of the HETFEM results to the analytical solutions for some cases of transient thermal conduction problem indicate good agreements between them.

To investigate the similarity of the non-nuclear rod to the fuel rod, thermal responses of a direct heater, indirect heater (FLECHT heater) and the 15×15 type fuel rod have been calculated by the HETFEM code. An assumed boiling curve has been applied to the boundary condition of them.

And, to investigate the clad-fuel gap effect on the thermal response, three gap conductance values of 500, 1000, 5000 kcal/m^2hr°C are selected for the fuel rod calculation.

The following conclusions are obtained from these calculations.

1) The FLECHT heater contains a little more stored energy than that of the fuel rod at the same initial condition of the reflood phase. And energy release rate near and below the quench front is much greater than that of the fuel rod due to the high thermal diffusivity of the insulator, boron nitride. These atipicalities affect the temperature response and canses delayed quench.

2) The direct heater inside of which is filled with magnesia oxide shows not exact, but similar thermal responses to those of the fuel rod, because low conductivity of the magnesia oxide acts like a gap thermal resistance in a fuel rod.

3) For the fuel rod, the value of the gap conductance affects directly the temperature response. The clad of the low gap conductance rod can be cooled down by releasing a small amount of the stored energy in the clad and also a small amount of the heat transfered from the fuel pellets. The residual stored energy is released gradually after the quench. Consequenty the sooner quench is observed for the lower gap conductance rod.

4) The heat releasing rate at near and below the quench front is affected by the thermal properties of the rod materials and the value of the pellet-clad gap conductance. The discrepancy of the heat releasing rate between the fuel rod and the simulator, or the fuel rods with different gap conductance value may affect the hydraulic behavior in the core which controls the precursory cooling, peak clad temperature and quench time. In the calculations, this effect was not considered due to utilize a simple assumed heat transfer curve in the code. Two dimensional calculation of which heat transfer model is related to the fluid conditions will be needed in the future. And experiments will be required to evaluate the gap effect on the precursory cooling and quench time.

Acknowledgement

The author is much indebted to Mr. Y. Murao for his guidance and encouragement for this study. I would like to express my appreciation to Dr. M. Nozawa, Head of Division of Reactor Safety, and to Dr. K. Hirano, Chief of Reactor Safety Lab. II. I also would like to express to thank Mr. N. Ohnishi for valuable discussions about HETFEM code development.

4) The heat releasing rate at near and below the quench front is affected by the thermal properties of the rod materials and the value of the pellet-clad gap conductance. The discrepancy of the heat releasing rate between the fuel rod and the simulator, or the fuel rods with different gap conductance value may affect the hydraulic behavior in the core which controls the precursory cooling, peak clad temperature and quench time. In the calculations, this effect was not considered due to utilize a simple assumed heat transfer curve in the code. Two dimensional calculation of which heat transfer model is related to the fluid conditions will be needed in the future. And experiments will be required to evaluate the gap effect on the precursory cooling and quench time.

Acknowledgement

The author is much indebted to Mr. Y. Murao for his guidance and encouragement for this study. I would like to express my appreciation to Dr. M. Nozawa, Head of Division of Reactor Safety, and to Dr. K. Hirano, Chief of Reactor Safety Lab. II. I also would like to express to thank Mr. N. Ohnishi for valuable discussions about HETFEM code development.

References

1) Murao, Y.,et al., "Report on Series 4 reflood experiment", JAERI-M 6982, Feb. 1977.
2) Ball, L.J., et al. "Semiscale program description", TREE-NUREG-1210, May 1979.
3) Cleary, W.F., et al., "FLECHT-SET phase B system design description", WCAP-8410
4) Reeder, D.L., "LOFT system and Test description (5.5 ft nuclear core 1 LOCEs)", NUREG/CR-0247, July 1978.
5) Varacalle, D.J. Jr., et al., "PBF/LOFT lead rod test series test results report", NUREG/CR-1538, July 1980.
6) Lemmon, E.C., "COUPLE - A pseudo finite element conduction code for the transient thermal response of aximmetric or plane anisothropic materials", SLC-RR-720324, Dec. 1972.
7) Slagter, W., et al., "TRIP a finite element computer program for the solution of convection heat transfer problems", RCN-243
8) Lewis, R.W., et al., "The determination of stresses and temperatures in cooling bodies by finite elements", Transactions of ASME, series E, pp.478-484, Aug. 1976.
9) Ohnishi, N., "HEATRAN-FEM : A finite-element conduction code for transient thermal response of the fuel rod in aximmetric and plane configrations", JAERI-M 6665, July 1976.
10) Emergy, A.F., et al., "An evaluation of the use of the finite element method in the computation of temperature", Transactions of ASME, series E, pp.136-145, May 1971.
11) Arpaci, V.S., "Conduction Heat Transfer", Addison-Wesley, Reading, Mass., 1966.
12) Portland General Electric Company, "Trojan nuclear plant final safety analysis report", DOCKET-50344-41
13) Sudo, Y., et al., "Film boiling heat transfer during reflood process", JAERI-M 6848, Dec. 1976.

Appendix

HETFEM Input Description

card 1 (FORMAT 7A10)

TITLE	

card 2 (FORMAT 12I6)

NNODW	total nodes number
NELEW	total elements number
NNHF	nodes number for heat flux boundary condition
NNHTG	elements number for heat generation
NEHG	nodes number for gap conductance
NNKNOW	known temperature nodes number
NUNKOW	unknown temperature nodes number
NBANW	matrix band width

card 3 (FORMAT 12I6)

RADSY ANGLE	} dimension of object
TEMPI TEMPIS	} initial temperature (option)
DIT	time increment
TIMEL	maximum calculation time

card 4 (FORMAT 12I6)

NDIV	number of X (r) axias division
NDIVA	number of Y axias division